

MULTI-PULSE BASED APPROACH
TO LIGHT SHEET MICROSCOPY

by

ZHANGATAY NUREKEYEV

Bachelor of Technics and Technologies, 2015
Al-Farabi Kazakh National University
Almaty, Republic of Kazakhstan

Submitted to the Graduate Faculty of the
College of Science and Engineering
Texas Christian University
in partial fulfillment of the requirements
for the degree of

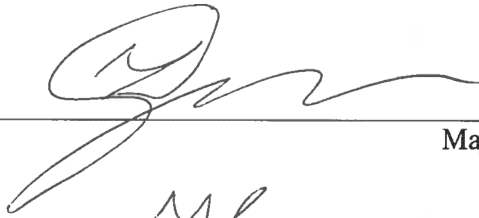
Master of Science

December 2018

MULTI-PULSE BASED APPROACH
TO LIGHT SHEET MICROSCOPY

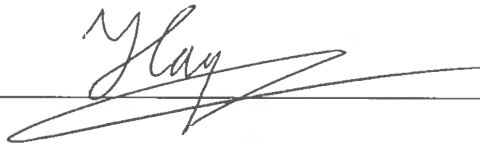
by Zhangatay Nurekeyev

Dissertation approved:

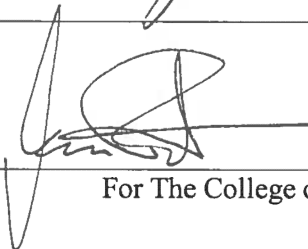
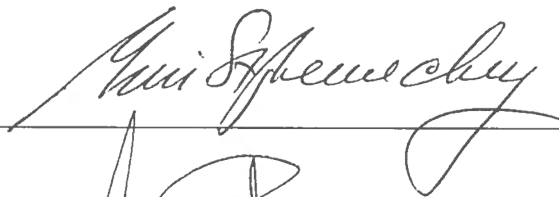


Major Professor

12105-118



Handwritten signature



For The College of Science and Engineering

Acknowledgments

I am very thankful to my scientific advisor Dr. Zygmunt (Karol) Gryczynski who has taught me many things including physics. I would like to express my gratitude towards my scientific committee members who have provided me with invaluable critique: Dr. Yuri Strzhemechny, Dr. Anton Naumov, Dr. Hana Dobrovolny.

Many thanks to Post-Docs and graduate program fellows, both present and past.

Table of Contents

Acknowledgments	ii
List of figures	iv
List of abbreviations	vi
1. Introduction	1
<i>1.1. Fluorescence Microscopy</i>	1
<i>1.2. Signal/Background</i>	5
<i>1.3. Phototoxicity/Photobleaching</i>	7
<i>1.4. Light Sheet Fluorescence Microscopy</i>	8
<i>1.5. Theoretical Model of Multi-Pulse Pumping</i>	13
<i>1.6. Concept for Time-Gated Detection</i>	15
<i>1.7. Multi-Pulse Pumping</i>	17
2. Experimental Setup	23
<i>2.1. Current Setup</i>	23
<i>2.2. Single Plane Illumination Microscopy</i>	25
<i>2.3. Multi-Pulse (Burst) Generator</i>	26
<i>2.4. Developing a Phantom Model</i>	27
<i>2.5. Image Acquisition and Analysis</i>	29
3. Results	30
4. Conclusions	35
5. Future works	37
References	40

VITA

ABSTRACT

List of figures

Figure 1.1.1. Jablonski diagram.....	2
Figure 1.1.2. The basic elements and geometry of an epifluorescence microscope.....	4
Figure 1.4.1. Light sheet illumination compared to other methods. ill – illumination, det – detection, LSFM – light sheet fluorescence microscopy, WF – widefield microscopy, CF – confocal microscopy.....	9
Figure 1.4.2. Common setup for light sheet illumination.....	10
Figure 1.4.3. A profile of a focused light beam near focal plane.....	11
Figure 1.5.1. Simulated intensity decays of a background and a probe.....	14
Figure 1.6.1. Excited state population at various gate opening time.....	16
Figure 1.7.1. Excited state population increase after 5 pulses at different Repetition rates.....	19
Figure 1.7.2. Excited state population change depending on lifetime/repetition rate ratio.....	20
Figure 1.7.3. Simulation of intensity decays of 3 dyes after 5 pulses.....	21
Figure 2.1.1. Experimental setup.....	23
Figure 2.3.1. Burst Generator concept.....	26
Figure 2.4.1. A phantom model.....	28
Figure 3.1. Intensity decay of a mixture of Rhodamine 110 and DAOTA in four pulse mode at 580 nm. Red rectangle represents the integration window.....	30

Figure 3.2. Time Resolved Emission Spectra of Rhodamine 110 and DAOTA mixture in one pulse and four pulse modes. Rhodamine 110 emission peak is at 523 nm, DAOTA peak is at 586 nm.....	31
Figure 3.3. Spectra of Rhodamine 110, DAOTA and recovered DAOTA (from TRES measurements).....	32
Figure 3.4. Images of PVA strips at different layers. First column contains images in one pulse mode. Second column contains images in four pulse mode. Third column is the recovered image by subtraction of results from previous two modes. Image size is 3325x3325 μm^2	34
Figure 5.1. Burst Generator realization through optical fiber bundle.....	37
Figure 5.2. Laser Array based Burst Generator.....	38

List of abbreviations

LSFM – light sheet fluorescence microscopy

SEM – Scanning electron microscopes

TEM – transmission electron microscopes

UV – ultra-violet

IR – infrared

CCD – charge-coupled device

ICCD – intensified charge-coupled device

ROS – reactive oxygen species

OPFOS – orthogonal-plane fluorescence optical sectioning

TLSM – thin light sheet microscopy

SPIM – selective plane illumination microscopy

WF – widefield microscopy

CF – confocal microscopy

RR – repetition rate

TCSPC – time correlated single photon counting

FWHM – full width at half maximum

PVA – polyvinyl alcohol

DAOTA – diazaoxatriangulenium

ADOTA – azadioxatriangulenium

Cys – cysteine

Met – methionine

Trp – tryptophan

Tyr – tyrosine

His – histidine

TRES – time resolved emission spectrum

1. Introduction

1.1. Fluorescence Microscopy

Microscopes have proven to be a powerful tool for studying a variety of phenomena/processes over many years. Around the 16th-17th centuries, the first compound optical microscopes were developed (Spottiswoode, 1876) (Helden, et al., 2010). Optical microscopes use visible light with a system of lenses to magnify an object and create an image with sub-micron precision. The fundamental lower limit of spatial resolution (due to diffraction of light on a finite aperture of an objective) predicted by Abbe in 1873 (Abbe, 1873) is around 200 nm for visible wavelength of light, a fact that has hindered optical microscopy for generations. Modern physics has greatly advanced the methods of microscopy since then. Scanning electron microscopes (SEM), transmission electron microscopes (TEM) and scanning probe microscopes were developed during the middle of the 20th century. TEM began to give better resolution than optical microscopes in 1933, dropping the limits to a nanometer scale, an achievement that was eventually awarded the Nobel Prize in Physics in 1986 (Knoll & Ruska, 1932). These methods now give angstrom resolution, but unfortunately would destroy biological samples limiting live science applications. In contrast, optical microscopy, especially fluorescence microscopy offers the possibility for non-destructive studies of biological systems with single molecule precision. Only in the early 2000's, optical microscopy was able to overcome fundamental limitations by applying a non-linear approach. This achievement earned the Nobel Prize in Chemistry in 2014 for Stefan Hell for super-resolution (Hell & Wichmann, 1994) (Klar & Hell, 1999) and Betzig and Moerner for single molecule detection (Moerner, 2006) (Betzig, et al., 2006). Presently, optical resolution can achieve 10 nm resolution and new methods are proposed that can lower it to a single nanometer. The dramatic advance in optical microscopy stimulated a lot of interest and new advances in

fluorescence optical microscopy has exploded in its variety of techniques and applications in recent decades.

Optical microscopes have developed intensively since the 16th century. Fluorescence microscopy started its development in the early 20th century with the first one invented in 1911 (Heimstädt, 1911) and for the last 30 years fluorescence microscopy has dominated biological fields. The approach utilizes the physical phenomenon of fluorescence – emission of light by a substance upon the absorption of light. The process is often described using a Jablonski diagram (Figure 1.1.1). Incoming electromagnetic radiation excites the molecule/atom from its ground state (S_0) to an excited state (S_1 , S_2). Then, an internal conversion to the lowest energy level of the first excited state (S_1) occurs (a process called relaxation). Afterwards, the single step transition to the ground state (S_0) releases a photon (emission of light). This transition to the ground state does not always have to be radiative, the energy may also be dissipated in a non-radiative way through heating or other energy transfer mechanisms.

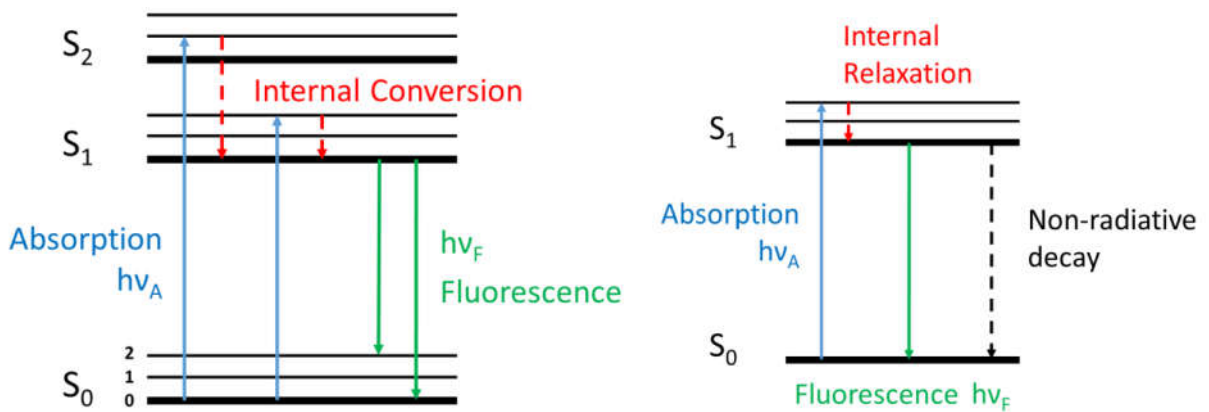


Figure 1.1.1. Jablonski diagram.

Because of the relaxation the fluorescence occurs at lower energy (longer wavelength) as compared to the energy of absorbed electromagnetic radiation (a phenomenon called Stokes shift).

The wavelength shift of fluorescence emission as compared to the absorption is a property that allows us to filter out the excitation light and observe only the emitted fluorescent signal without the excitation light background. This property leads to enhanced sensitivity as compared to other techniques (e.g. contrast microscopy, or electron microscopy) allowing even single-molecule detection (Moerner & Fromm, 2003). Maximum absorption and emission wavelengths are defined by the substance itself and its environment and usually is in the optical range of UV, Visible, and near-IR light. Since the transition from excited state to the ground state is a statistical (probabilistic) process, the fluorescence intensity decay of the excited state population typically is an exponential function with the exponent parameter describing the excited state population called the fluorescence lifetime. Fluorescence lifetime is the time after which the population of excited molecules decreases e -times (where e is the base of natural logarithm ~ 2.72).

Fluorescence microscopy requires the specimen to be fluorescent. Certain molecules and atoms can be fluorescent. They are usually called fluorophores or fluorescent dyes. Typically, organic molecules containing aromatic rings are fluorescent. Such fluorophores are sensitive to their micro-environment and can be used as a label for tracking biological processes. Proper choice of filters allows one to distinguish the fluorescence signal and observe only fluorophores that label very specific elements of a sample (targeted labelling), giving high specificity. Since only the fluorescence signal is observed, the contrast of imaging is significantly better compared to other optical microscopy techniques. However, many aromatic structures commonly contained in biological structures may exhibit their own fluorescence, overlapping with label emission. Such fluorescence will typically constitute a background signal in fluorescence microscopy.

A basic fluorescence microscope consists of multiple elements: a light source, a set of filters, an objective, a specimen holder, an ocular and a detector. The light source is used to excite

fluorophores within the sample, so its wavelength must overlap with the absorption wavelengths of the fluorophore. The beam from the light source (excitation beam) passes through the excitation filter

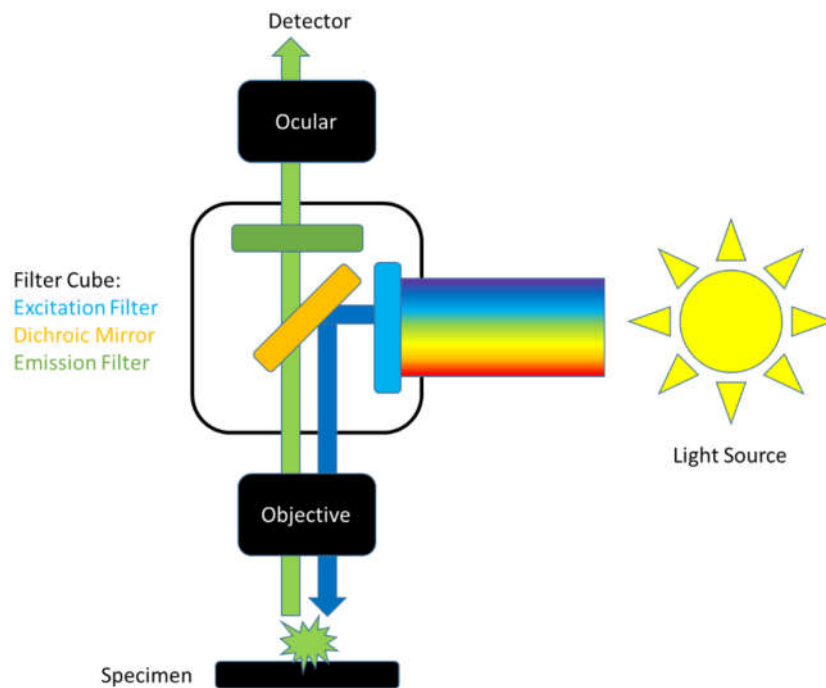


Figure 1.1.2. The basic elements and geometry of an epifluorescence microscope.

within the filter cube. This excitation filter is needed to select only those wavelengths that are absorbed by the label (specimen). A dichroic mirror then reflects the beam towards the objective and then to the specimen. The spectral characteristics of the dichroic mirror are chosen so that the excitation beam is reflected and fluorescence emission from the sample is transmitted. The objective focuses the excitation beam onto a region of interest and magnifies the image of fluorescence emission. The emission filter is chosen so that the remaining (leaking) excitation beam doesn't pass through it and only emission wavelengths are transmitted. It is very important to make sure that transmittances of excitation and emission filters are not overlapping, otherwise

a leak of the excitation beam through the emission filter may distort the image and in some cases damage the detector.

Various detectors can be used. Usually these are single-point detectors for scanning microscopes (avalanche diodes, photo-multiplier tubes etc.) or charge-coupled device (CCD) cameras. The image is acquired by scanning with a point excitation the sample and detecting point-by-point image or illuminating the sample and detecting simultaneously a whole field using a CCD camera.

Figure 1.1.2 describes the geometry of elements for an epifluorescence microscope where the excitation and emission beams are aligned along the line. It is the most commonly used composition for fluorescence microscopy.

1.2. Signal/Background

The typical experiment involving a fluorescence microscope requires a high signal from a species of interest and low background. However, very often the background signal is significantly overlapping with the fluorescence signal. The problem of background remains very important in fluorescence imaging (Frangioni, 2009). It is the case for living cells and other in vitro measurements with high-sensitivity detectors. Cells contain fluorescent molecules that can be excited with UV/Vis radiation. Proteins in tissue often contain tryptophane, tyrosine and other amino acids which are fluorescent, as well as melanin, flavins and many other substances in biological samples. All of these intrinsic fluorophores combined contribute to autofluorescence – natural emission of light by biological structures upon absorption of light (Monici, 2005). Intrinsic

fluorophores are abundant in biological systems and have significant presence in cellular imaging. It is not possible to get rid of intrinsic fluorophores without physically altering the sample, therefore, other means are necessary to reduce background.

Other sources of background are Rayleigh scattering of light (elastic scattering of electromagnetic radiation by particles that are much smaller than the wavelength) which can be easily eliminated by proper choice of cleaning optical long-pass/band-pass filters, Raman scattering (inelastic scattering of electromagnetic radiation by molecules) can be eliminated with proper choice of notch filter since it has very narrow wavelength distribution ($\sim 5\text{nm}$). Also, isolation of a sample from stray light from room light is necessary to reduce background signal. In the case of epi-fluorescence microscopy out-of-focus fluorophores contribute to background due to the geometry of epi-illumination.

Signal-to-Background ratio could be increased if the signal from the labeling dye was higher, but modern dyes are already near the theoretical limit of brightness of fluorescent dyes.

There are methods to reduce background analytically, where background signal from homogenous media is calculated and subtracted from images (Soubret & Ntziachristos, 2006). But the method requires a complex imaging technique, pre-experimental data, and homogeneous distribution of intrinsic fluorophores, which is a reasonable assumption for large biological samples with low spatial resolution, e. g. small animal imaging.

There is a way to reduce the background signal with proper timing of observation. It is to use either time-gated detection or time gated analysis. Biological samples possess a significant amount of intrinsic fluorophores, so when excited we observe a signal coming from both the fluorophore of interest along with the background signal.

One important property of autofluorescence that we can utilize is that it has very short lifetime, usually ~3 nanosecond and below. By choosing a fluorophore with a relatively longer lifetime, e.g. 20 nanoseconds, we can temporally separate autofluorescence from the actual signal coming from a desired fluorescent dye. This is possible because the signal of the short-lived autofluorescence will decay before long-lived fluorophore decays. So by opening the detector shutter after a small delay, this will cut off the first few nanoseconds of measurements which are dominated by the unwanted background signal. This technique is known as time-gated detection.

1.3. Phototoxicity/Photobleaching

Phototoxicity is the result of significant light exposure of biological cells. It may happen that cells will experience light-induced damage that alters their physiology and, therefore, affects the experimental results. In fluorescence microscopy, high intensity illumination is typically used to excite the fluorophore-labeled cells. This high intensity of light can cause the production of light-induced reactive oxygen species (ROS) that leads to photooxidative damage. ROS production can affect cell physiology in two possible ways: it can directly damage proteins, lipids and nucleic acids within cells and/or it can perturb redox homeostasis (reduction-oxidation balance). The effect is more dramatic during extended measurements (Dixit & Cyr, 2003). For example, singlet oxygen ($^1\text{O}_2$) is generated by UV/visible light in the presence of sensitizer. Particularly, proteins, Cys, Met, Trp, Tyr and His side chains are major targets for $^1\text{O}_2$ since they are abundant in biological systems and have high reactivity rates (Wright, et al., 2002).

Photobleaching is a process in which a fluorescent molecule permanently loses its ability to fluoresce due to photon-induced damage. Upon transition from an excited singlet state to the excited triplet state, fluorophores might interact with another molecule to produce irreversible covalent modifications. The triplet state is relatively long-lived with respect to the singlet state, thus allowing excited molecules a much longer timeframe to undergo chemical reactions with components in the environment. The average number of excitation and emission cycles that occur for a particular fluorophore before photobleaching is dependent upon the molecular structure and the local environment. Some fluorophores bleach quickly after emitting only a few photons, while others that are more robust can undergo thousands or millions of cycles before bleaching.

1.4. Light Sheet Fluorescence Microscopy

The roots of light sheet fluorescence microscopy come from a technique called ultramicroscopy which was developed in 1902 by Richard Adolf Zsigmondy and Henry Siedentopf (Siedentopf & Zsigmondy, 1902). The original ultramicroscope focused sunlight from the side of colloidal gold solutions, with the resultant scattering detected orthogonally to the plane of illumination. Zsigmondy was awarded the Nobel Prize in Chemistry in 1925 for this work. However, this method didn't achieve much popularity at the time. The first fluorescence microscope with side illumination came in 1993 when Arne Voie and David Burns introduced orthogonal-plane fluorescence optical sectioning (OPFOS) microscopy that was applied towards imaging and mapping the guinea pig inner ear cochlea (Voie, et al., 1993). In 1995, Ernst H. K. Stelzer and Steffen Lindek combined orthogonal illumination with scanning confocal microscopy

– confocal theta microscopy, which resulted in higher axial resolution (Stelzer, et al., 1995). In 2002, Eran Fuchs and colleagues applied thin light sheet microscopy (TLSM) towards imaging unperturbed aquatic microenvironments (Fuchs, et al., 2002). In 2004, the Stelzer group modified his technique using planar light sheets and widefield detection, thus, introducing selective plane illumination microscopy (SPIM) (Huisken, et al., 2004). From that moment LSFM gained huge popularity and started to rapidly develop.

Light sheet fluorescence microscopy is gaining a spot in the very demanding world of modern biology. Its advantages compared to conventional optical microscopy techniques include: reduced light exposure of a sample, true depth resolution, selective plane illumination, and the possibility of widefield detection.

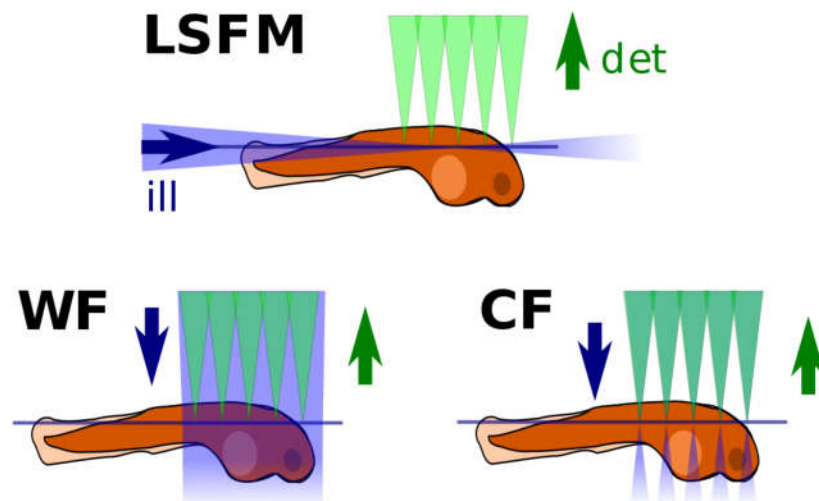


Figure 1.4.1. Light sheet illumination compared to other methods. ill – illumination, det – detection, LSFM – light sheet fluorescence microscopy, WF – widefield microscopy, CF – confocal microscopy (Krieger, 2013).

Photobleaching and phototoxicity occur upon repeated exposure of a sample to lasers or other light sources. Widefield illumination excites fluorophores at multiple layers of a sample (Figure 1.4.1) even though the focal plane of an objective is a thin, single layer. In this case, out-of-focus signal from adjacent layers also is observed as blurry spots in the image, which then contribute to a non-homogeneous background. Confocal microscopy uses a pinhole in order to eliminate out-of-focus fluorescence, but still significant non-observed part of a sample is illuminated with laser. In the case of light sheet illumination, the laser beam comes from the side in the form of a thin slice. In this case, only a thin slice of the sample is illuminated, and fluorescence emission occurs only in that very layer. This geometry allows us to achieve true depth-resolution if layer is not larger than the focal plane's thickness of the observing objective. Since only a thin slice of the sample that is observed is illuminated, light exposure to the sample is reduced, which leads towards reduced phototoxicity and photobleaching. This advantage of LSFM suits very well to prolonged experiments, such as observation of plant development or embryogenesis.

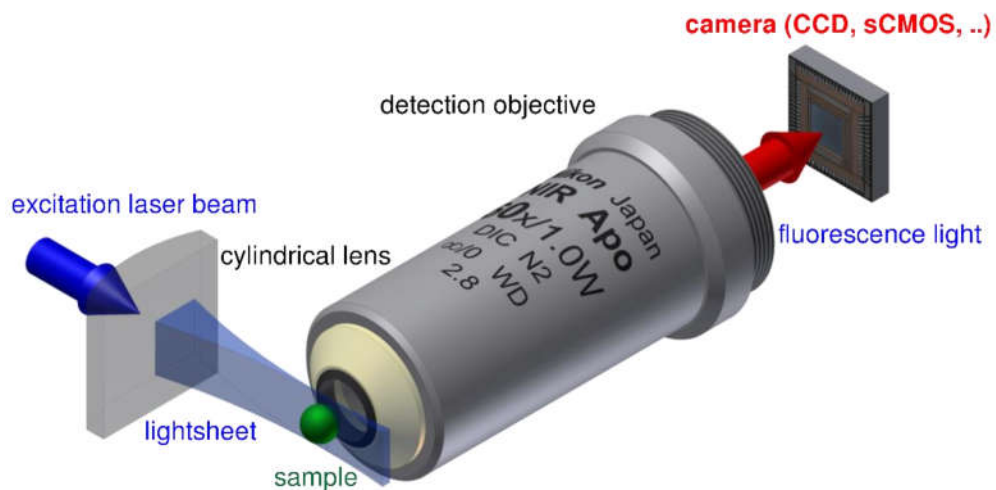


Figure 1.4.2. Common setup for light sheet illumination (Krieger, 2012).

A typical setup for light sheet fluorescence microscopy (Figure 1.4.2) is rather simple. The laser beam is guided through a cylindrical lens which converges the light onto a static planar sheet. This method of creating a light sheet is called selective plane illumination microscopy (SPIM). The objective's focal plane crosses the excitation focal plane in order to observe the thinnest layer possible. The best suitable detection system is a camera rather than a single-point detector because a wide area is illuminated.

Another approach of creating a light sheet is scanned light sheet where the beam is focused using a spherical lens and then scanned through the sample to form a sheet. This method is slower than SPIM and requires precise beam movements to form a sheet instead of a static cylindrical lens.

A typical light source used in LSFM is a laser. The light beam's cross-section intensity distribution can be controlled with different types of lenses used to form a light sheet: approximately Gaussian beam with cylindrical lens, Bessel beam with axicon (conical shaped lens) etc. Axicons do not converge light onto a sheet, so they can be used only for Scanned Light Sheet. We are using a cylindrical lens for its ability to form a whole sheet and the relative simplicity of the setup.

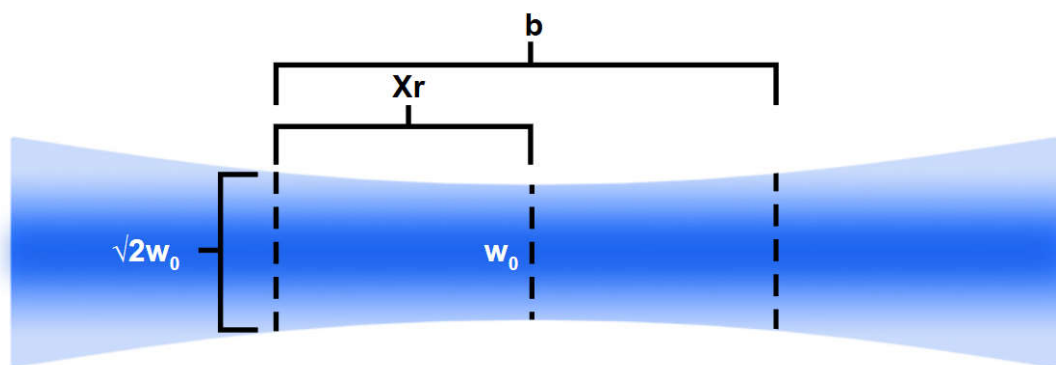


Figure 1.4.3. A profile of a focused light beam near focal plane (Allen, 2018).

A perfectly planar sheet is impossible to create. In Figure 1.4.3 a profile of a Gaussian beam around a focal plane travelling from left-to-right (or vice versa) is shown. The thickness of a layer is:

$$\omega_0 = \frac{1.4f\lambda}{2D_{lens}} \quad (1)$$

where ω_0 – sheet thickness, f – focal length of illumination optics, λ – wavelength of the illumination light, D_{lens} – diaphragm of illumination optics. Often a beam-expander is used in front of a laser in order to increase beam size which can further decrease sheet thickness. Also a mask can be used in order to cutoff parts of the beam with significantly lower intensity compared to the center of the beam.

The distance through which the sheet can be said to provide near-homogenous planar illumination is defined by the confocal parameter, which is twice the Rayleigh range – the distance from the center to where the beam center has thickened by a factor of $\sqrt{2}$ in one direction:

$$b = 2X_R = \frac{2\pi\omega_0^2}{\lambda} \quad (2)$$

where b – confocal parameter, X_R – Rayleigh range.

If the beam travels through a medium with refractive index n :

$$b_n = 2nX_R = bn \quad (3)$$

A common problem with LSFM is the presence of striping artifacts. These artifacts are the result of single-direction illumination. Any scattering, absorbing elements of a sample perturb the initial part of the incident beam resulting in weaker illumination at the end of the beam. It causes visible stripes on the image. A possible solution is multi-view imaging where the sample is rotated

and subsequently the images at different angles are overlapped. Also it is possible to illuminate the sample from multiple angles simultaneously, which allows the sample to remain stationary, but the complexity of a setup is significantly higher.

Sample preparation differs from that of epifluorescence illumination. Thickness of a sample must be larger than that of a light sheet. Since a larger part of a sample is observed simultaneously in case of single plane illumination, the sample has to be more transparent.

Generally, LSFM is compatible with most of the current fluorescence microscopy techniques such as confocal microscopy, super-resolution microscopy etc.

1.5. Theoretical Model of Multi-Pulse Pumping

The detected signal from a sample is the sum of photons emitted by the probe's molecules as well as all other background photons reaching the detector. This background includes contributions from excited endogenous chromophores, scattered photons that pass through the filter system, Raman scattering, and other minor contributors. What limits the detection is the ratio between the signals from the probe and from the background. This ratio is typically independent of the excitation power. Because of that fact, research efforts were focused on increasing the fluorophore brightness (extinction coefficient and quantum yield) for many years. After many decades, multiple dyes have been developed that approach theoretical limits for the extinction coefficient ($\sim 200,000$), close to 100% quantum yield, but very short (nanosecond) fluorescence lifetime. Also a high extinction coefficient and high quantum yield dictates that the spectral Stokes' shift is very small (10 nm – 20 nm), thus putting the excitation wavelength and detection

wavelength very close. This adversely impacts the scattering contribution and the background still remains the limiting factor. Especially because physiological samples by principle cannot be purified.

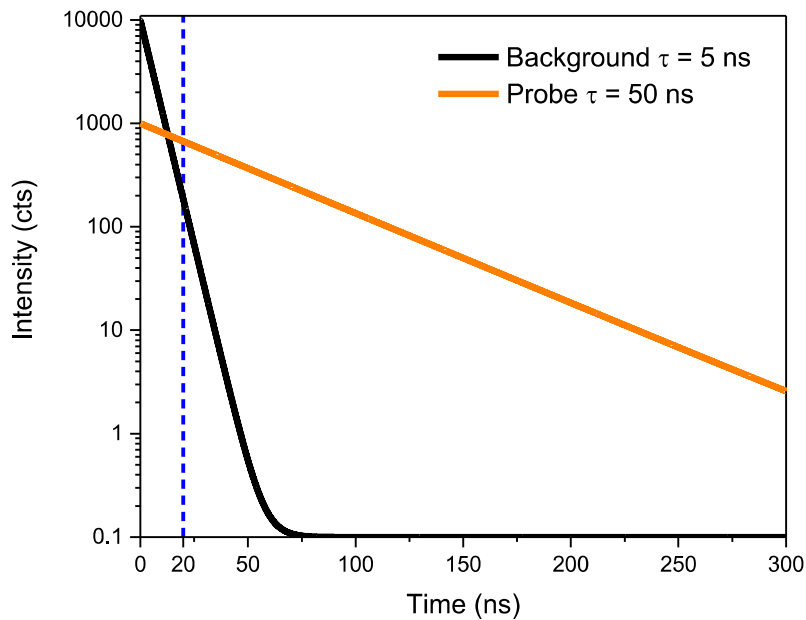


Figure 1.5.1. Simulated intensity decays of a background and a probe.

We recently realized that a much more appropriate way for handling physiological samples would be to limit the background contribution by designing a new experimental approach. Fluorescence lifetimes of most physiological components contributing to the background (e.g. flavines, porphyrin degradation components, etc.) are short-lived, typically below 5 ns and frequently even in the sub-nanosecond range. The scattering background (both direct and Raman) is instantaneous, thus contributing only during the pulse duration. The overall background is characterized by a short fluorescence lifetime and for the last 20 years, researches were trying to use longer lifetime dyes in connection with time-gated detection. The simple concept for time

gated detection is to excite the sample with a very short pulse, wait for a certain time for all of the background to decay and then open (switch-on) the detector. This waiting time is called the time gate delay, and should be significantly longer than the fluorescence lifetimes of all background components.

1.6. Concept for Time-Gated Detection

Consider a sample that is characterized with a background average fluorescence lifetime of 5 ns and the sample is labeled with a fluorophore that has a fluorescence lifetime of 50 ns. Assume the sample is excited with a very short laser pulse (δ -pulse). Most current laser pulses would be in the range of 100 fs – 100 ps, which is much shorter than the background fluorescence lifetime. Let us assume that the steady-state intensity measured out of the sample is 100 and it is 50% background contribution and 50% probe signal. Typically, such a measurement would be disqualified because of the background. In Figure 1.5.1 we present intensity decays for the background component and the probe signal. The initial signal (signal at time zero) from the probe is much lower (10 fold) than the signal from the background, so integrated over time intensities (steady-state intensities) are equal. In Figure 1.5.1, we also marked a gate opening time of 20 ns. At 20 ns the intensity of the steady-state probe signal decreases to 67% of initial value, while the background signal decreases to only 1.8% of its original value. Figure 1.6.1 shows relative steady-state intensities that would be observed after different delays (10 ns, 20 ns, 30 ns) for different gate opening times (different delay times). Already 10 ns gives a significant advantage for the probe signal. For a 20 ns gate delay, the signal from the probe decreased only 33% while from the

background 98.2% and the signal from the probe constitutes 97.3% of overall signal. And for a gate of 30 ns, the signal of the probe drops to 55% while the probe signal constitutes 99.6% of overall detected signal. This are excellent improvements that makes measurement of the probe practically free of background.

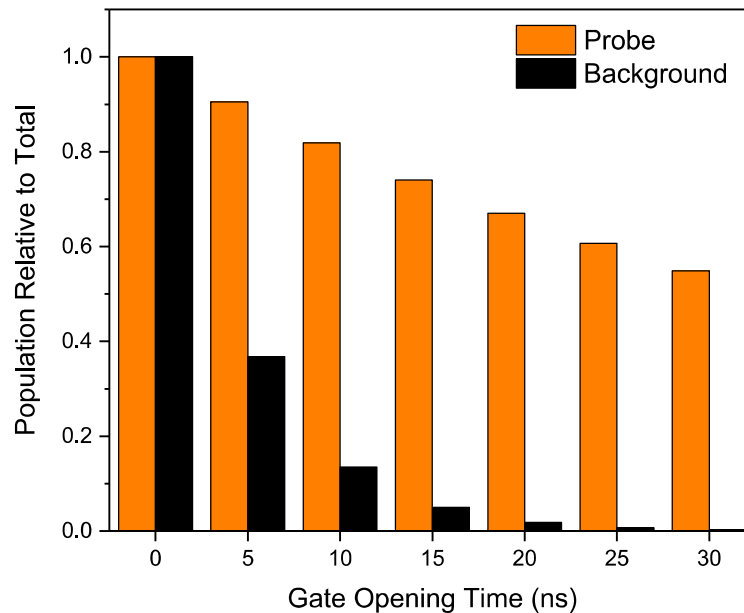


Figure 1.6.1. Excited state population at various gate opening time.

With such great improvements, one would ask the question why time-gated detection is not used very commonly. Especially since recent progress in electronics and detector design allows easy nanosecond time gate manipulation. There are a few important factors that are limiting time-gating applications:

- First, time-gating is a passive approach that always results in signal lost.
- Second, most probes that have longer fluorescence lifetimes inherently have a lower extinction coefficient (<10,000) and lower quantum yield (<10%). So, the brightness of the

probe is low, thus requiring high labelling concentration that is not suitable for physiological applications.

- Third, most known long-lived probes are on the order of microsecond (metal-ligand probes) and millisecond (lanthanide probes). These are very low brightness probes but the gating is very effective. However, to gate milliseconds, the laser repetition must be very low making the detection speed very slow.

1.7. Multi-Pulse Pumping

Recently we realized that we could increase apparent signal from lower brightness, long-lived dyes when using a burst of pulses. Typical fluorescence experiments are performed under the condition where only a very small fraction of the fluorescent molecules are excited. This is also true for most of the imaging/detection systems using high power (tens of mW range) picosecond pulsed diode lasers focused by the objective to a small excitation spot. For example, a 1 mW power focused to a 10 femtoliter volume will still excite much less than 1% of available fluorophores. Our goal is to exclusively increase the population of excited long-lived probes without increasing the population of the short-lived background.

The repetition rate (RR) used in time correlated single photon counting (TCSPC) systems is usually determined by the fluorescence lifetime of the dye. To avoid problems in data analysis, the time between pulses ($1/RR$) should be 5-10 times longer than the fluorescence lifetime of the longest lifetime component of the sample. Otherwise the fluorescence decay after a particular pulse would overlap with that of the subsequent pulse. Hence for a typical decay time for a background of less than 5 ns, a RR of 40 MHz (25 ns between two consecutive pulses) is sufficient

for the background's excited state to decay completely. However, if we consider a fluorophore that will have a fluorescence lifetime of 100 ns the population of excited state between two consecutive pulses will decay only to 77.7% and after the second pulse the population of excited dyes would be much greater than after the first pulse.

Now let us consider the case when the RR is not sufficiently low to allow the complete decay after each excitation pulse. The number of fluorophores in the excitation volume (in the beam) is N_0 and a single pulse excites N_e molecules ($N_e \ll N_0$). The observed fluorescence intensity (signal) is proportional to the number of molecules excited by each pulse ($I \sim N_e$). This situation changes when the RR approaches a level such that subsequent pulses arrive before the excited population can decay completely. Since $N_0 \gg N_e$, we can assume that depletion of the ground state by each individual pulse is negligible and each pulse excites N_e molecules. Such a system will reach equilibrium when the number of molecules excited by a single pulse is equal to the number of molecules that return to the ground state over the time interval equal to $1/RR$. So for a given RR, the number of excited molecules returning to the ground state between pulses is simply the difference between the total number of molecules in the excited state immediately after the pulse's arrival, $N_e(T)$, and the total number of molecules in the excited state after time $1/RR$ (the time when the next pulse arrives):

$$N_e = N_e(T) - N_e(T) * e^{-\frac{1}{\tau * RR}} = N_e(T)(1 - e^{-\frac{1}{\tau * RR}}) \quad (4)$$

One can also calculate the number of molecules in the excited state by analyzing subsequent pulses. The first pulse excites N_e molecules. When the second pulse arrives, the number of molecules remaining in the excited state is $N_1 = N_e * e^{-\frac{1}{\tau * RR}}$ and the total number of excited molecules immediately after the second pulse is $N_e^1 = N_1 + N_e$. Extending this for n

pulses we have a geometrical series, and the number of molecules in the excited state after n pulses will be:

$$N_e(T)^n = N_e * (1 - e^{-\frac{n}{\tau * RR}}) / (1 - e^{-\frac{1}{\tau * RR}}) \quad (5)$$

And consequently for an infinite number of pulses:

$$N_e(T) = N_e / (1 - e^{-\frac{1}{\tau * RR}}) \quad (6)$$

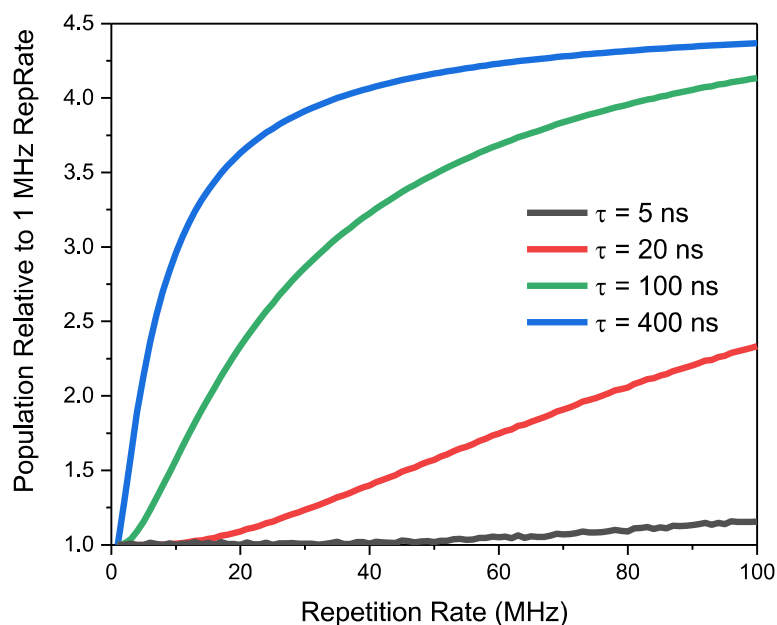


Figure 1.7.1. Excited state population increase after 5 pulses at different repetition rates.

That is identical to the equilibrium solution given by Equation 4. In Figure 1.7.1 we present the number of excited molecules after 5 pulses for four model fluorophores with fluorescence lifetimes of 5 ns, 20 ns, 100 ns, and 400 ns as function of increasing the RR from 1 MHz to 100 MHz. It is intuitive that the number of molecules in the excited state after each pulse for a short-lived fluorophore is constant and for a long-lived fluorophore it increases quickly with the RR. It

is important to realize that for a continuous train of pulses, the outcoming intensity of fluorescence (number of emitted photons) depends on the decay factor $e^{-\frac{1}{\tau*RR}}$ and relative intensities for short-lived and long-lived fluorophores increase proportionally with increasing RR. The intensity is not only proportional to the number of molecules in the excited state at the instant of each excitation pulse, but also to the interval between pulses. This is obvious since in steady-state conditions the relative intensities must be the same—increasing the RR cannot change the relative signals of the two fluorophores.

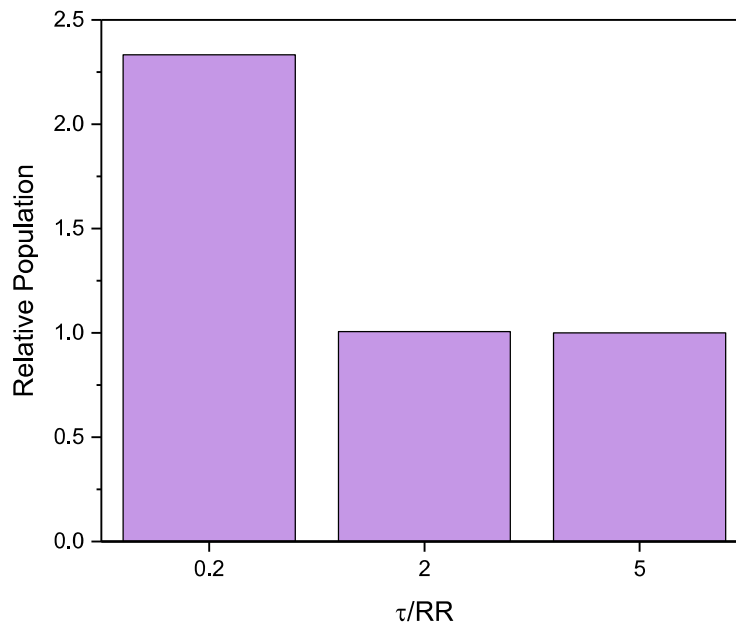


Figure 1.7.2. Excited state population change depending on lifetime/repetition rate ratio.

However, this situation changes dramatically when we use a different approach. With technology available today, we can use variable pulse trains that allow time for the excited states to depopulate completely after a series of pulses (burst of pulses). For example, 80 MHz RR in the burst and burst RR of 500 kHz (separation between two consecutive bursts of 2,000 ns) will allow

us to collect a complete decay for lifetimes below 500 ns. Then, by detecting only the fluorescence decay after the last pulse in the burst, we can dramatically change the relative intensities of long-lived probes. Depending on the ratio between the fluorescence lifetime, τ and $1/RR$ (time between two consecutive pulses) the initial population of the excited state will be different, thus resulting in a different number of photons collected after the last pulse in the burst as shown in Figure 1.7.2 for $\tau/RR = 0.2, 2,$ and 5 ns respectively.

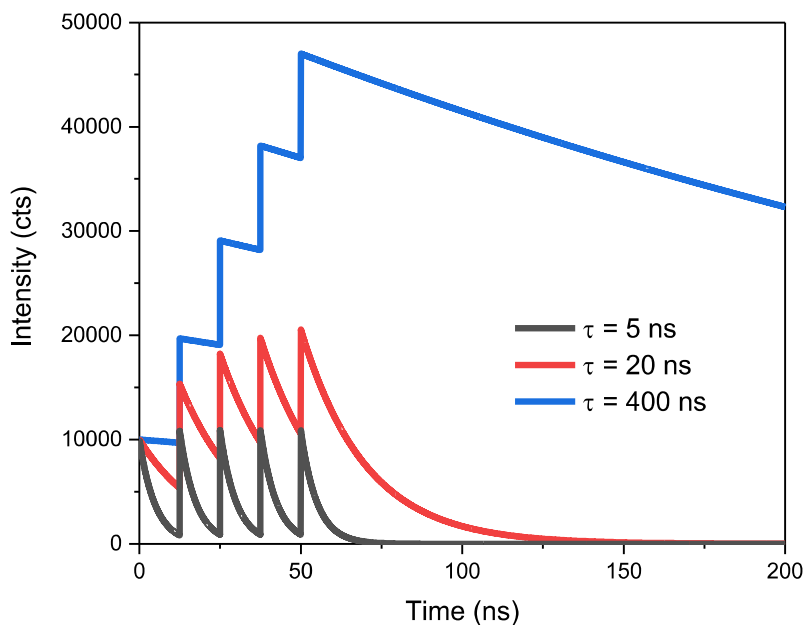


Figure 1.7.3. Simulation of intensity decays of 3 dyes after 5 pulses.

For example, Figure 1.7.3 models the fluorescence decay of three fluorophores with 5 ns, 20 ns, and 400 ns lifetimes excited by 5 excitation pulses arriving with a RR of 80 MHz (12.5 ns between pulses). The total fluorescence from each dye over the time interval shown will be the result of exactly 5 excitation-decay cycles, regardless of whether these cycles are completed or not. For the 5 ns dye, the decays are almost completely between excitation pulses and each cycle is

practically completed, but for the 20 ns we can see significant signal enhancement and for the 400 ns the population of excited fluorophores increases over 4 times. If we only measure the fluorescence decay after the last excitation pulse, this measurement for the 20 ns and 400 ns dyes will include the overlapping excited state population from previous excitation pulses in the burst. Thus it is this break between excitation bursts of pulses that we may exploit in order to increase the contrast between fluorophores of differing decay times (or a short-lived background). It is easy to see that for a fixed RR in the burst, an increased lifetime results in a greater relative signal for the long-lived dye. For fluorescence lifetimes much longer than the separation of pulses in the burst ($1/RR$), the number of long-lived fluorophores in the excited states for small number of pulses in the burst is proportional to that number of pulses. So, for a repetition rate in the burst of 80 MHz (typically highest RR for pulsed laser) and a dye with fluorescence lifetime of 100 ns or more (like some metal-ligand complexes) the number of dyes in the excited state after, for example, 5 pulses is ~ 5 times greater than for a single pulse. At the same time, the number of background fluorophores at the excited state that have fluorescence lifetime of 2 ns will be almost constant from pulse-to-pulse (the fluorophores will decay completely within a 12.5 ns interval time). In effect synchronizing the time correlated detection with the last pulse in the burst will give ~ 5 times greater signal than that from each individual pulse. We also want to stress that this is conceptually very different from using lower repetition single pulses but 5 times stronger. For 5 times stronger pulses both populations (short-lived background and long-lived dye) increases proportionally (5 times in this case).

2. Experimental Setup

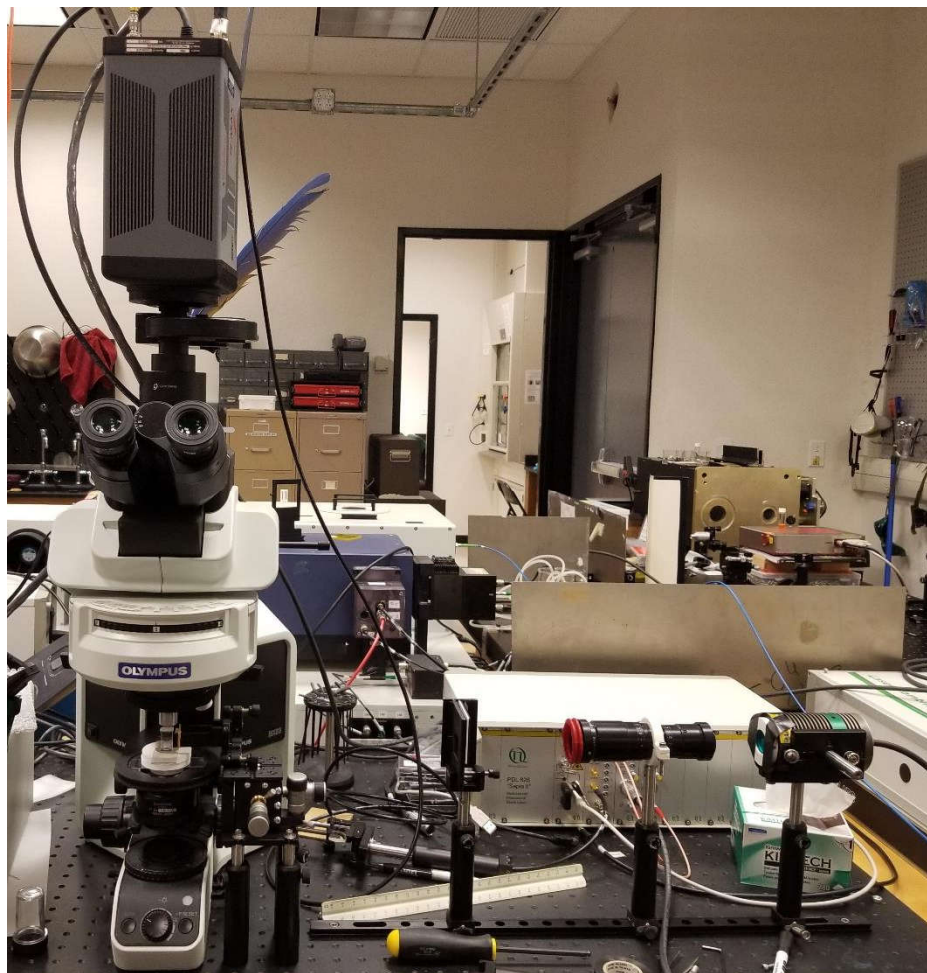


Figure 2.1.1. Experimental setup.

2.1. Current Setup

The experimental setup (Figure 2.1.1) contains many elements. The microscope frame is Olympus BX53. It is an upright fluorescence microscope. A filter wheel and a camera were attached to it for the experiment. The stage of the microscope can be moved vertically in order to bring the desired layer of a sample into the focal plane of an objective. The minimal movement

step of the stage is 1 μm . A dry objective with 4x magnification is used for collecting the fluorescence signal from a sample. Since the objective and laser beam are static and their focal planes are aligned, only the movement of a sample is necessary to scan the sample vertically. The excitation filter attached in front of the laser is a band-pass interference filter. It transmits only from 450 nm to 500 nm. a dichroic filter cuts out below 562 nm. The emission filter is a band-pass interference filter that transmits only from 570 nm to 613 nm.

The light source is a pulsed laser system. It is made up of two elements: a laser driver from PicoQuant – PDL 828 “Sepia II” and a laser head from PicoQuant – LDH P-C-485. The laser driver sends trigger signals to both laser head and the camera. It has three main frequencies: 80 MHz, 64 MHz and 50 MHz. So, the maximum frequency available is 80 MHz, which means the separation between light pulses is 12.5 ns. Even though there are only three fundamental frequencies, the output trigger signal sequences can be altered and various trigger signal patterns can be generated. Also, trigger signal sequences to the laser head and camera are not necessarily the same. The wavelength of the laser head is 485 nm. The time distribution of a laser pulse is described by its full width at half maximum (FWHM), in which this case is less than 110 ps.

The detection system is an intensified CCD camera (ICCD) from Princeton Instruments – PI-MAX4 1024f. It has a time-gating ability and 10 picosecond time resolution. It allows us to collect data only at desired time windows, specifically after the last pulse within the burst by delaying its acquisition window after the trigger signal. The resolution of the camera is 1024x1024 pixels. The size of a single pixel is 13.0x13.0 μm^2 . The active area of the detector is 13.3x13.3 mm^2 . Since we used a 4x objective the area that camera is observing is 3325x3325 μm^2 . The camera acquisition windows are triggered by the laser driver signal

2.2. Single Plane Illumination Microscopy

From the multiple techniques of light sheet microscopy, we have chosen single plane illumination microscopy. It is relatively easy to set it up and perfectly matches the ability of our ICCD camera to time-gate the acquisition of a fluorescence signal. The optical element that converges the light beam into a sheet is a cylindrical lens.

This laser beam's spatial intensity is similar to that of a Gaussian distribution. Therefore, the center of the light sheet intensity is significantly stronger than at its edges. In order to improve the homogeneity of the light sheet, we would like to use only the central part of the beam where its intensity distribution is relatively constant. First, we use a beam expander that is installed in front of the laser. A beam expander is an optical device that expands the size of a collimated beam. We set it to expand the beam 5 times. Second, a mask with an opening of *height* = 1 mm and *width* = 5 mm is used in order to cut out the edges of the beam and allow only the center of the expanded beam to pass through it. This way the homogeneity of a light beam is increased.

A cylindrical lens with a focal length = 10 mm is used to form a light sheet. The lens is mounted on a customized holder made with a 3D-printer. The holder is then mounted on a kinematic mirror/lens mount Thorlabs KM100. It controls the angular position of a lens. Then the mount is attached on a Thorlabs MBT616. 3-axis stage with 1 um movement precision. This allows the control of the lateral position of a lens.

All of these elements are aligned along the line and the beam is focused on the sample. Taking into account all the parameters, the thickness of a layer is $\omega_0 = 3.395 \text{ um}$, while the confocal parameter in a medium of refractive index 1.5 is $b_n = 223.866 \text{ um}$.

2.3. Multi-Pulse (Burst) Generator

A typical time-resolved fluorescence measurement is accomplished using a pulsed laser. The pulse of light excites fluorescent molecules in a sample and then their emission intensity decay is observed in time. The time period between pulses is chosen so that the fluorophore completely decays before the next pulse arrives. If the next pulse arrives before the sample's emission has completely decayed, then the population of fluorescent molecules increases. Depending on the time delay between pulses and the lifetime of a fluorophore, one can achieve a significant increase of the excited state population, hence enhancing the emission intensity.

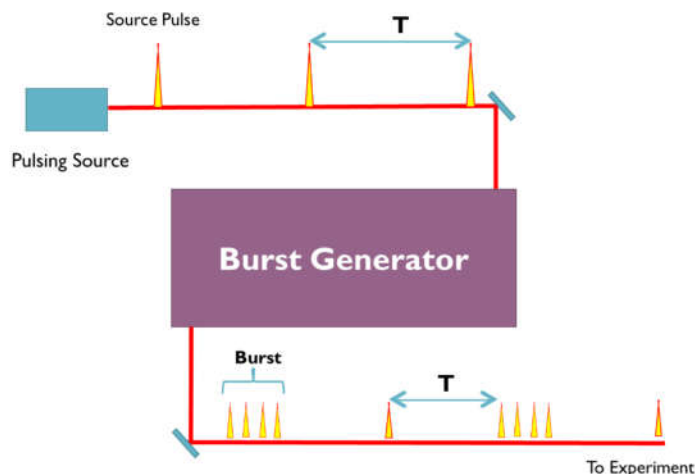


Figure 2.3.1. Burst Generator concept.

An important part of the approach is the Burst generator. It creates a special pattern of light pulses as shown in Fig. 2.3.1. A conventional pulsed light source with a constant time delay between pulses is converted into series of bursts and single pulses. The time delay between pulses within a burst is shorter than the time delay between bursts and a single pulse. The easiest way to achieve a burst is to use modern laser drivers that can create a desirable pattern of pulses. Commercially available laser drivers allow time delays up to 12.5 nanosecond between pulses. It's

enough to increase the excited state population of fluorophores with lifetimes of ~100 nanoseconds and more. This is another reason for our choice of dyes. With the laser driver available to us, one can send a trigger signal to the camera every 100 ns and send five trigger signals to the laser head with 12.5 ns separation every 100 ns. So, the time window between repeated signal sequences is 100 ns. In this case, within 100 ns one trigger signal to the camera and five trigger signals to the laser head are sent. Five trigger signals with 12.5 ns separation take 50 ns to complete. Therefore, the first 50 ns of the time window are filled with trigger signals while the remaining 50 ns of the time window are empty. Of course, the regular mode with one trigger pulse to both the laser head and the detector are also possible if desired.

2.4. Developing a Phantom Model

In order to imitate a case of an experiment with a biological substance, a “phantom” model has been developed. This phantom possesses the characteristics of a typical biological sample. It is easier to reproduce and work with phantom models rather than with biological substances when acquiring a proof of concept. Figure 2.4.1 shows the phantom model developed for this experiment.

The fluorescent elements are polyvinyl alcohol films embedded with fluorescent dye. Two dyes were used: Rhodamine 6G and Ruthenium. These dyes were chosen since they have very different lifetimes and are bright compared to other dyes with similar lifetimes. Also, both dyes absorb significantly at 485 nm and their emission spectra largely overlap. They were separately mixed with an aqueous solution of 10% PVA and then dried for one day under ambient conditions. As a result, two films were produced: one with Rhodamine 6G and one with Ruthenium. Then thin

slices of films were cut. In the experiment, three strips were used: two with Rhodamine 6G and one with Ruthenium. The lifetime of Rhodamine 6G in PVA is 5.0 ns. The lifetime of Ruthenium in PVA is 1.7 μ s. The lifetimes were measured using the time-resolved spectrofluorometer PicoQuant FT300 in front-face geometry.

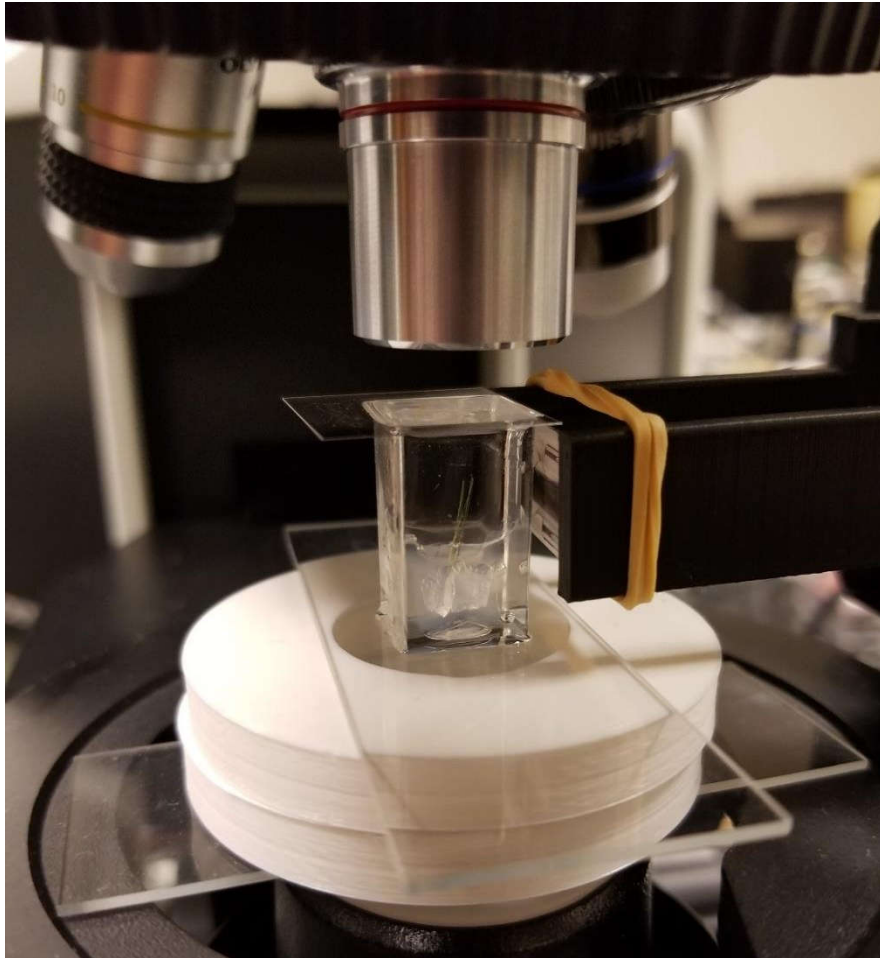


Figure 2.4.1. A phantom model.

Due to the high refractive index of PVA film ($n = 1.50$) compared to air, the fluorescence light from a sample will be highly distorted on film-air interfaces. In order to reduce this mismatch, the PVA strips were embedded in a medium of similar refractive index. Mineral oil has been chosen for this purpose. Its refractive index is close to that of a PVA film ($n = 1.46$) and also is

transparent in the visible range of light spectrum. In order to hold them together, a transparent plastic cuvette was filled with gel glue up to half of the cuvette. Then the PVA strips were embedded into gel so that they are standing still. Then the top half of the cuvette is filled with mineral oil. Since the mineral oil will form a meniscus on top of the cuvette (or a little under it), the cuvette was covered with a glass slide. Now all the surfaces of a phantom are flat (the cuvette surface for the excitation beam and the glass slide surface for the emission beam).

2.5. Image Acquisition and Analysis

The time window of repetitive pulse sequences was set to 2,000 ns. This window was chosen since there is no fluorescence signal at the end of this window. The images were acquired in two modes: one pulse and four pulses. In one pulse mode, the acquisition starts right when the laser pulse arrives. In four pulse mode, the acquisition of the fluorescence signal starts when the last pulse within the burst arrives. The separation between pulses within the burst is 50 ns, so the total duration between the first pulse and the fourth pulse is 150 ns. Therefore, the acquisition window must be less than $2,000 - 150 = 1,850$ ns. That is why we have chosen the acquisition window equal to 1,800 ns. In this case, the acquisition window is no longer than the time duration between the last pulse in a burst and the beginning of a new sequence of pulses. To gain enough signal, 3×10^6 pulse sequences were collected for each image. The sample was moved vertically in order to image different layers. 101 layers with 10 μm separation were imaged.

Images acquired during the experiment were analyzed using ImageJ software. The images in one pulse mode were subtracted from the images in four pulse mode.

3. Results

In order to check if the method works as intended, a regular cuvette measurement was performed using PicoQuant FT300. Two fluorescent dyes with different lifetimes and small spectral overlap were chosen: Rhodamine 110 with 4.0 ns lifetime and emission wavelength peak at 523 nm, DAOTA with 20.0 ns lifetime and emission wavelength peak at 586 nm. The intensity decays of a mixture of these dyes were measured in two modes: one pulse and four pulse. Pulse separation in case of four pulse mode was 3 ns. It was achieved using a custom fiber with four optical paths of different length. Only the signal from DAOTA is enhanced when pumping with four pulses. Excitation laser wavelength is 485 nm.

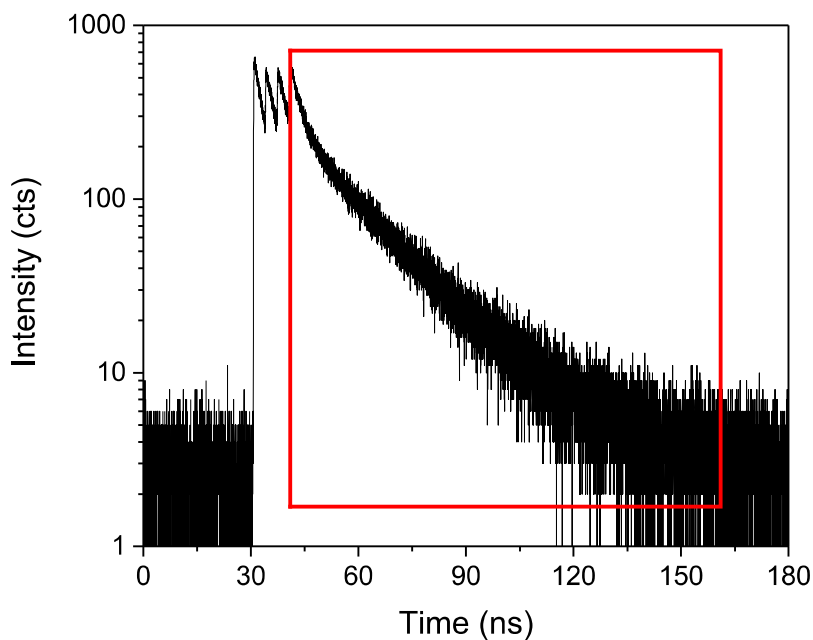


Figure 3.1. Intensity decay of a mixture of Rhodamine 110 and DAOTA in four pulse mode at 580 nm. Red rectangle represents the integration window.

Intensity decays are measured at different wavelengths. Then decays are integrated to get the total intensity at a given wavelength. By plotting total intensity at given wavelength versus the wavelength the spectra of the sample were reconstructed. This method is called time resolved emission spectrum (TRES). It is important to note that not the whole decay was integrated. Integration begins with the last pulse within the burst in case of four pulse mode (or with the pulse in case of one pulse mode). The integration window (similar to acquisition window, but it is data manipulation rather than electronically controlled accumulation of light within set windows) is 120 ns (example is shown on Figure 3.1).

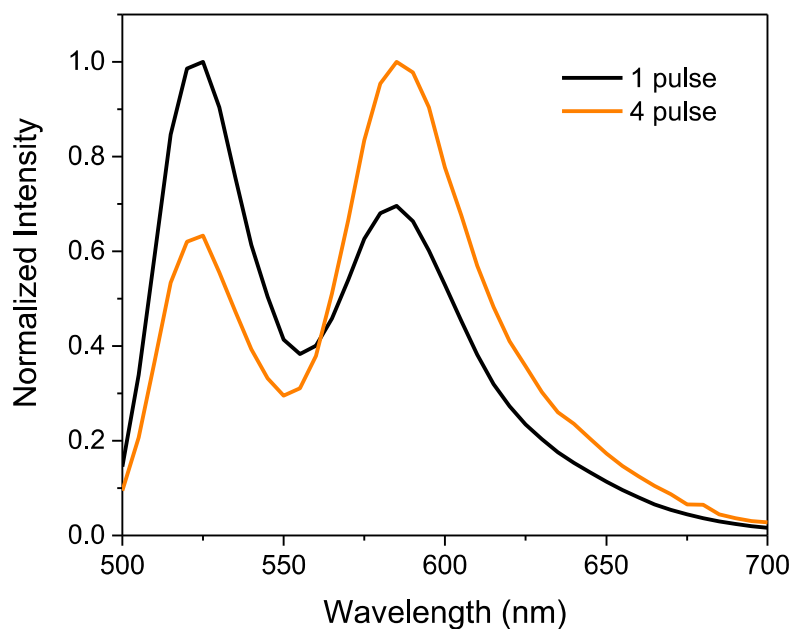


Figure 3.2. Time resolved emission spectra of Rhodamine 110 and DAOTA mixture in one pulse and four pulse modes. Rhodamine 110 emission peak is at 523 nm, DAOTA peak is at 586 nm.

TRES were measured in one pulse and four pulse modes (Figure 3.2). It is notable that intensity ratios in the two modes are significantly different. This is due to the pumping of the

excited state population of DAOTA. Upon subtraction of these spectra we were able to recover the spectrum of DAOTA only.

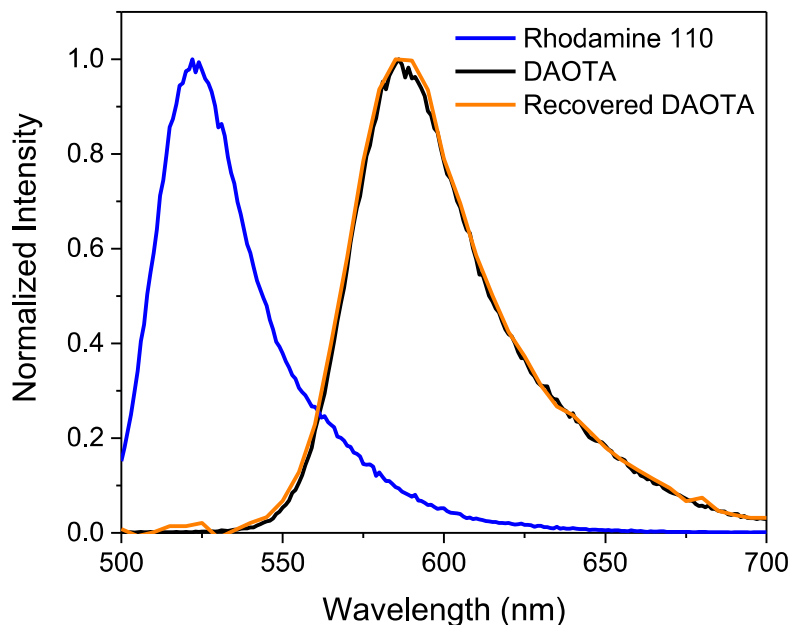


Figure 3.3. Spectra of Rhodamine 110, DAOTA and recovered DAOTA (from TRES measurements).

Then we compared recovered spectrum of DAOTA to spectra of non-mixed Rhodamine 110 and DAOTA (Figure 3.3). One can easily see that the spectrum of DAOTA is near perfectly recovered. Thus, Rhodamine 110, which imitated the short living background, was eliminated from the spectrum.

Then we imaged PVA strips with embedded fluorescent dyes. The experiment is described in Chapter 2. 101 slices were image with 10 μm separation between layers. So, 1 mm of a sample is scanned.

Looking at the images (Figure 3.4) acquired in one pulse mode it is not apparent which signal is from the long living dye and which is from the short living dye. However, when the same layer of a sample is imaged in four pulse mode, it is easy to notice that some elements of an image are enhanced. PVA films with Ruthenium are enhanced through multi-pulse pumping. Bright circular spots in the images are out-of-focus fluorescence signal. Even though light sheet illumination has significantly reduced out-of-focus light, significant amount of it still remains.

The image that is the result of subtraction of images in four pulse and one pulse modes (the third column of Figure 3.4) is recovered image of long-lived component. Since only the long-lived component of a sample was enhanced, the short-lived component is almost completely eliminated upon subtraction. This method allowed us to get rid of non-homogenous background with short lifetime, as well as homogeneous background with short lifetime or homogeneous constant background. Homogeneous constant background is contributed by dark counts of a detector. In contrast with the fluorescence signal it is invisible, but the counts of it were reduced to nearly 0. Absolute elimination of background is impossible due to the thermal detector noise at each pixel. To summarize, we were able to identify PVA strips that contained Ruthenium using multi-pulse pumping.

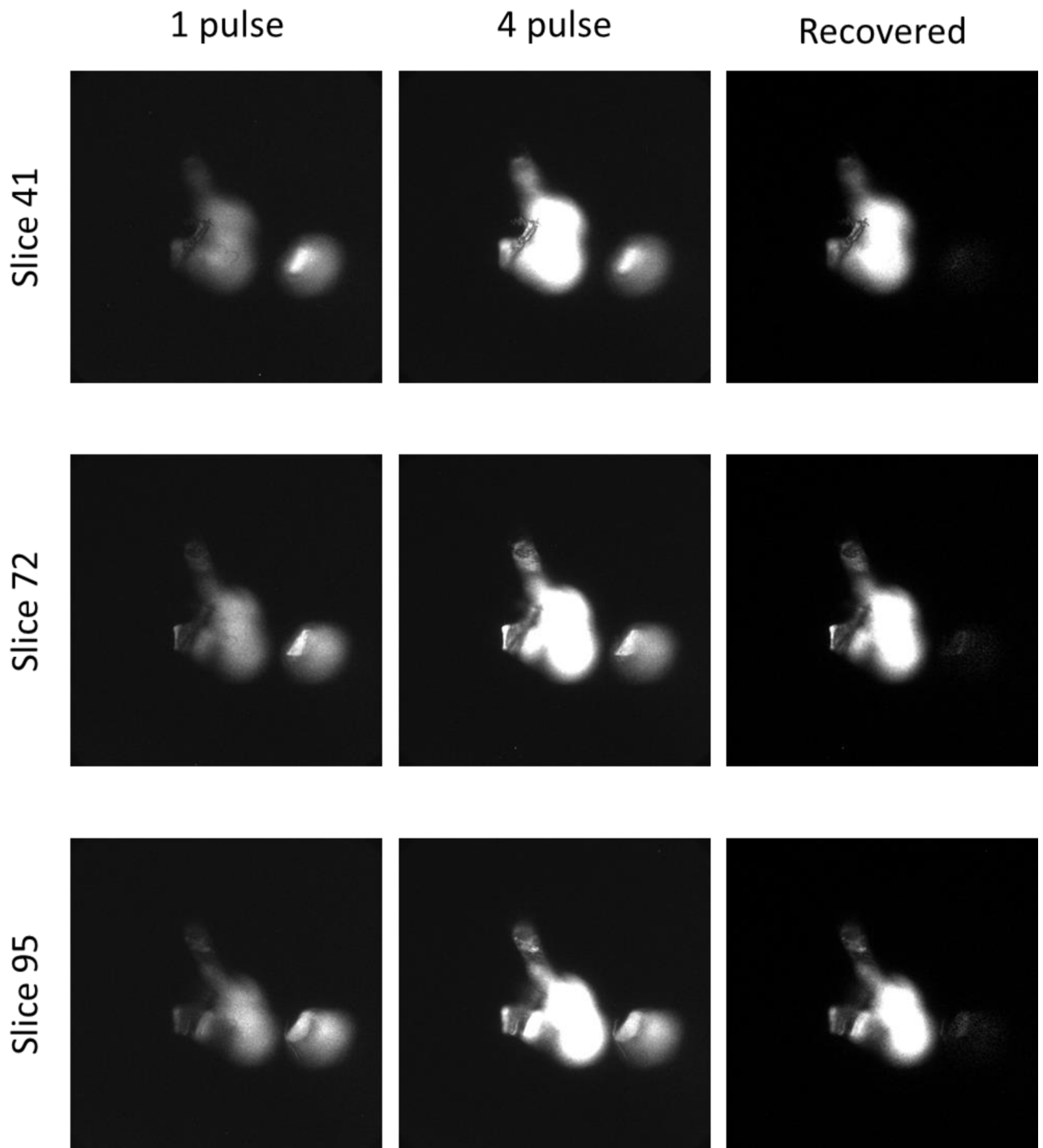


Figure 3.4. Images of PVA strips at different layers. First column contains images in one pulse mode. Second column contains images in four pulse mode. Third column is the recovered image by subtraction of results from the previous two modes. Image size is 3325x3325 μm^2 .

4. Conclusions

In this work we showed that the method of multi-pulse pumping allows us to collect background free images. One pulse mode replicates a regular fluorescence imaging experiment, while multi-pulse mode enhances only the long living components of a sample. Since autofluorescence is rather short living (lifetimes are less than 5 ns), and there are available dyes with significantly longer lifetimes, it is possible to use this method in biological fluorescence imaging. After the subtraction of images, non-homogeneous short living background is almost completely eliminated. Homogeneous background is eliminated as well. It is an advantage compared to mathematical methods of background elimination which require prior knowledge of spatial distribution of autofluorescence sources for non-homogeneous background. While subtraction of images decreases total signal, our results indicate less than 50% loss. In principal, as long as lifetime of a dye is longer than that of an autofluorescence, it is possible to selectively enhance excited state population of long living fluorescence dye. Practically, our method requires lifetime of a labeling dye to be a few times longer than that of a background fluorescence. Since typical autofluorescence lifetime is shorter than 5 ns, dyes with 15 ns and longer are suitable for the multi-pulse pumping method. Such dyes need short pulse separation within a burst, and commercially available laser drivers allow only 12.5 ns separation. Thus, new strategies for generating short pulse separations are necessary in order to reach a limit of multi-pulse pumping method. Possibility of using such short living dyes is the main advantage compared to time-gated detection, which is useful when lifetime of a dye is in microsecond range. Thus, background free imaging with higher speeds than currently available is achievable with our method. Further work is needed to reach the limits of a method, including minimal label concentration needed for

pumping. Imaging of biological samples with dyes meeting our requirements is already possible with our multi-pulse pumping method.

The method can be implemented in any laboratory that has equipment for time-resolved fluorescence imaging. Commercially available laser drivers can achieve up to 12.5 ns separation between pulses which is sufficient to pump dyes with lifetime of 100 ns or more. Common detectors used in fluorescence lifetime imaging microscopy techniques can be easily used due to their high time resolution. There are a few cameras with sub-nanosecond resolution.

Multi-pulse pumping is compatible with various fluorescence techniques. In this work it was used for intensity decay measurements and for light sheet fluorescence microscopy.

5. Future works

Image acquisition times depend on the lifetime of a dye. The shorter the lifetime shorter the acquisition windows. Modern laser drivers are useful to pump dyes with lifetimes of 100 ns or more. So, in order to increase imaging speed (which allows us to observe faster biological processes) we are working on creating light bursts with pulse separation less than 12.5 ns. Dyes with a lifetime of about 20 ns (DAOTA, ADOA etc.) can be pumped with pulse separation of 3 ns. There are multiple ways to generate such pulses. One way this can be achieved is on an optical table using beam splitters so that part of a single pulse goes directly onto a sample and other part passes through another system of beam splitters to create a burst.

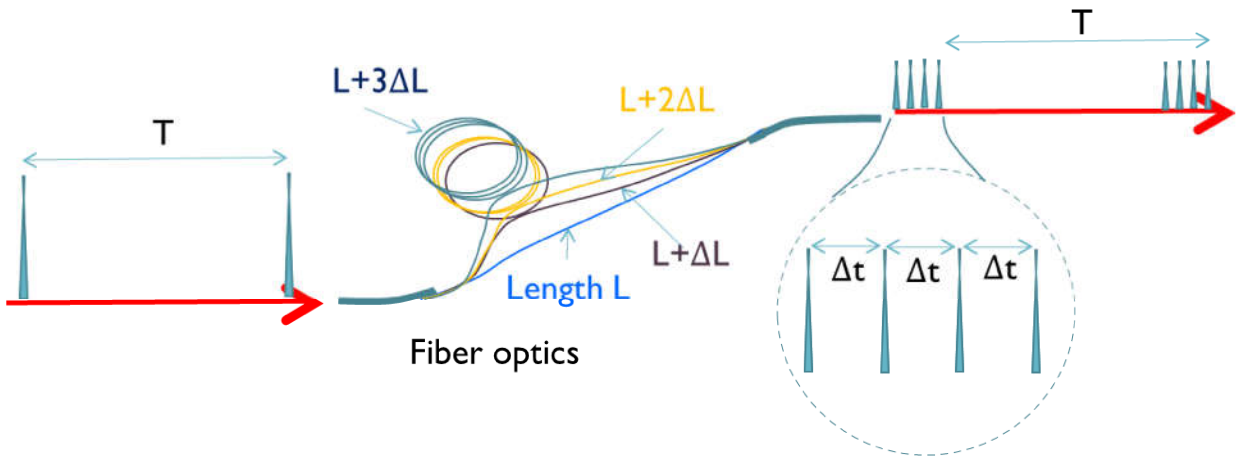


Figure 5.1. Burst Generator realization through optical fiber bundle.

Another method to create a burst generator is using an optical fiber that splits the beam into multiple beams (Figure 5.1). Such fiber is made out of a bundle of fibers where each of them have different lengths. We have a fiber with 4 different lengths. Difference in lengths causes delay between output beams. 90 cm of difference causes 3 nanosecond delay between beams, which is ~ 4 times shorter than on commercially available laser drivers. Each beam travels a different

distance, thus, after converging the beams, creating a burst. We have utilized this bundle to pump DAOTA previously for measurements of intensity decays, but there are certain problems with implementing it as a light source for a microscope. Since it is a bundle of fibers, illumination from a bundle is far from homogeneous.



Figure 5.2. Laser array based burst generator.

We would like to create a burst generator that is based on a laser array (Figure 5.2). If one combines 2 or more identical lasers in an array and couples them into a single fiber, such system can be used as a burst generator. Laser drivers can control up to 8 lasers simultaneously, and lasers respond to triggering signal coming from a laser driver. By altering the length of the cable for the triggering signal one can create a needed pattern of pulses. This is desired method since it has greater flexibility compared to fiber bundle.

In this experiment we were manually switching between single pulse mode and multi-pulse mode. Automation of switching and synchronization of it with the detector would definitely increase imaging speeds.

References

- Abbe, E., 1873. Beiträge zur Theorie des Mikroskops und der mikroskopischen Wahrnehmung. *Archiv für mikroskopische Anatomie*, 9(1), pp. 413-418.
- Allen, J. R., 2018. *Light Sheet Fluorescence Microscopy*. [Online]
Available at: <https://www.microscopyu.com/techniques/light-sheet/light-sheet-fluorescence-microscopy>
- Betzig, E. et al., 2006. Imaging intracellular fluorescent proteins at nanometer resolution. *Science*, 313(5793), pp. 1642-1645.
- Dixit, R. & Cyr, R., 2003. Cell damage and reactive oxygen species production induced by fluorescence microscopy: effect on mitosis and guidelines for non-invasive fluorescence microscopy. *The Plant Journal*, 36, pp. 280-290.
- Frangioni, J. V., 2009. The Problem is Background, not Signal. *Molecular Imaging*, Vol 8, No 6, pp. 303-304.
- Fuchs, E., Jaffe, J., Long, R. & Azam, F., 2002. Thin laser light sheet microscope for microbial oceanography.. *Optics express*, 10(2), pp. 145-154.
- Heimstädt, O., 1911. Das Fluoreszenzmikroskop. *Z. Wiss. Mikrosk.*, 28, pp. 330-337.
- Helden, A., Dupré, S. & Gent, R., 2010. The Origins of the Telescope. *Amsterdam University Press*, pp. 32–36, 43.
- Hell, S. & Wichmann, J., 1994. Breaking the diffraction resolution limit by stimulated emission: stimulated-emission-depletion fluorescence microscopy. *Optics Letters*, Vol 19, Issue 11, pp. 780-782.
- Huisken, J. et al., 2004. Optical sectioning deep inside live embryos by selective plane illumination microscopy.. *Science*, 305(5686), pp. 1007-1009.
- Klar, T. & Hell, S., 1999. Subdiffraction resolution in far-field fluorescence microscopy. *Optics Letters*, Vol 24, Issue 14, pp. 954-956.
- Knoll, M. & Ruska, E., 1932. Das elektronenmikroskop. *Zeitschrift für physik*, 78(5-6), pp. 318-339.
- Krieger, J., 2012. [Online]
Available at: https://en.wikipedia.org/wiki/File:Spim_prinziple_en.svg
- Krieger, J., 2013. [Online]
Available at: https://en.wikipedia.org/wiki/File:Lsfm_lightsheetinsample.svg
- Moerner, W. E., 2006. Single-molecule mountains yield nanoscale cell images. *Nature Methods*, 3, pp. 781-782.
- Moerner, W. E. & Fromm, D. P., 2003. Methods of single-molecule fluorescence spectroscopy and microscopy.. *Review of Scientific Instruments* 74.8, pp. 3597-3619.

- Monici, M., 2005. Cell and tissue autofluorescence research and diagnostic applications. *Biotechnology annual review*, 11, pp. 227-256.
- Siedentopf, H. & Zsigmondy, R., 1902. Über sichtbarmachung und größenbestimmung ultramikroskopischer teilchen, mit besonderer anwendung auf goldrubingläser.. *Annalen der Physik*, 315(1), pp. 1-39.
- Soubret, A. & Ntziachristos, V., 2006. Fluorescence molecular tomography in the presence of background fluorescence. *Physics in Medicine & Biology*, 51(16), p. 3983.
- Spottiswoode, W., 1876. Physics News. *Nature*, May 18, pp. 54-56.
- Stelzer, E. et al., 1995. A new tool for the observation of embryos and other large specimens: confocal theta fluorescence microscopy.. *Journal of microscopy*, 179(1), pp. 1-10.
- Voie, A., Burns, D. & Spelman, F., 1993. Orthogonal-plane fluorescence optical sectioning: three-dimensional imaging of macroscopic biological specimens.. *Journal of microscopy*, 170(3), pp. 229-236.
- Wright, A., Bubb, W. A., Hawkins, C. L. & Davies, M. J., 2002. Singlet Oxygen-mediated Protein Oxidation: Evidence for the Formation of Reactive Side Chain Peroxides on Tyrosine Residues. *Photochemistry and photobiology*, 76(1), pp. 35-46.

VITA

Personal

Zhangatay Rashiduly Nurekeyev

Education

Certificate of Average General Education, 2011
School-Gymnasium №122
Almaty, Republic of Kazakhstan

Bachelor of Technics and Technologies, 2015
Al-Farabi Kazakh National University
Almaty, Republic of Kazakhstan

Professional Experience

2012-2015 – Laboratory Assistant, Laboratory of Cryophysics and
Cryotechnologies, Al-Farabi Kazakh National University

2016-Present – Graduate Teaching Assistant, Texas Christian University

ABSTRACT

MULTI-PULSE BASED APPROACH TO LIGHT SHEET MICROSCOPY

by Zhangatay Nurekeyev, 2018
Department of Physics & Astronomy
Texas Christian Univeristy

Thesis Advisor: Zygmunt (Karol) Gryczynski, Professor of Physics and "Tex" Moncrief Jr. Chair

Optical microscopes have proven their use as a powerful tool for studying biological samples. In spite of many successful applications there are still many obstacles limiting microscopy applications. Besides the resolution limitation, background and probe toxicity are two main aspects limiting many potential applications. Any new method that would allow an increase in signal-to-background ratio and at the same time reduce probe photobleaching and phototoxicity would immediately allow many new investigations like, for example, studying long lasting processes such as embryo development, cancer drug delivery, or plant growth.

In our approach, we combine a technique called single plane illumination microscopy (SPIM) with multi-pulse pumping in order to enhance the signal-to-background ratio and at the same time reduce light exposure times for the specimen. To test applicability and limits of the new technology, we developed a phantom model containing various probes and an artificial background.